Optical design, fabrication and evaluation of optical systems using free-shaped prism

H. Ohde and T. Nagata

OLYMPUS CORPORATION, 2-3 Kuboyama-cho, Hachioji-shi, Tokyo 192-8512, Japan

ABSTRACT

Free-shaped optical systems can highly correct aberrations by reflecting light at multiple aspherical surfaces inside a prism and can realize more-compact, higher-performance optical systems than is normally achievable. We have exploited these features at Olympus to construct optics for display systems and image-capturing modules in mobile phone cameras. In the course of their development, we improved the accuracy of the finished form of free-shaped prisms by establishing a design methodology for free-shaped optical systems and developing high-precision fabrication and measurement techniques. In this paper, we describe the structure and characteristics of an optical system for an image-capturing module, as well as evaluation results of a prototype that we fabricated.

Keywords: free-shaped prism, optical systems, evaluation, shape error, decentering, ultra-compact camera modules

1. INTRODUCTION

At Olympus, we have been developing free-shaped optical elements and have been investigating their applications in various fields. Features of free-shaped prisms include their ability to fold the optical path inside the prism and their ability to highly correct aberrations by reflecting the light at multiple aspherical surfaces. As a result, they allow realization of compact, high-performance optical systems.

By exploiting these features, in 1998 we commercialized a head-mounted display (HMD) called Eye-Trek, the world's first display optical system using free-shaped prisms [1]. In an HMD, a large virtual screen can be observed by magnifying and projecting a compact display element with an optical system, as shown in Fig. 1(a). With this optical system, a liquid crystal display with 180,000 pixels is magnified and projected using a prism including free-shaped surfaces. An image equivalent to a 62-inch screen at a distance of 2 m can be viewed. For higher resolution, a system combining the same type of free-shaped prism with a diffractive optical element (DOE) has also been introduced (Fig. 1(b)). With this design, chromatic aberrations caused by the free-shaped prism are corrected with the DOE [2].

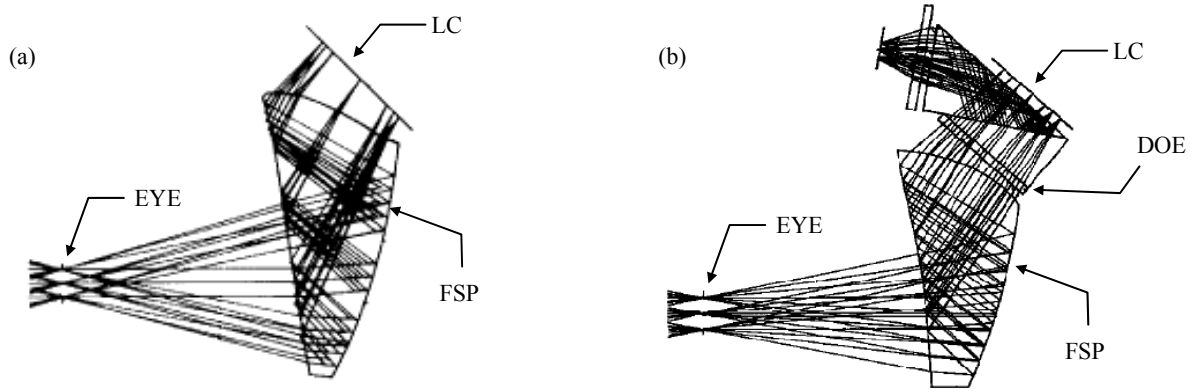

Fig. 1 Optical system using free-shaped prism for a head mounted display. (a) single prism type, (b) high resolution type using DOE, LC: liquid crystal display device, FSP: free-shaped prism, DOE: diffractive optical element.

Optical Design and Testing III, edited by Yongtian Wang, Theo T. Tschudi, Jannick P. Rolland, Kimio Tatsuno
Proc. of SPIE Vol. 6834, 68340K, (2007) · 0277-786X/07/$18 · doi: 10.1117/12.757395

Use of free-shaped surfaces in image-capturing optical systems is promising because of their ability to reduce the size, even for conventional coaxial optical systems using aspherical surfaces. As a target application exploiting this feature, we focus on image-capturing modules for mobile-phone cameras. The resolution of these image-capturing modules has been rapidly increasing in recent years, and at the same time, there has also been a trend towards more compact modules in response to demands for mobile phones with greater portability and more attractive designs, resulting in the need for both compactness and high performance.

Looking at the market for image-capturing modules, since 2001 when CIF-class image-capturing modules (110,000 pixels) started to be built-into mobile phones, the resolution has dramatically increased. In 2004 for instance, camera mobile phones with 3 megapixels class image-capturing modules were available. Along with this trend, the number of lenses has also increased, from one in CIF-class modules, to lenses in VGA-class modules (330,000 pixels) and lenses in megapixel-class modules, inevitably resulting in thicker camera modules.

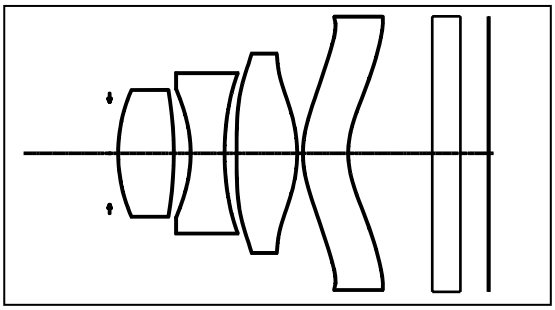

Fig. 2 Co-axial Optical system for a camera module having 2 to 3 mega-pixels.

Fig. 2 shows an example optical design for a module of the 3 megapixel class or above. To ensure a practical level of image quality using an image-capturing device with 3 megapixels or above, in the case of a coaxial system described above, three or four lenses are required, which limits the reduction in thickness of the optical system that can be achieved. One design means for reducing the thickness of the optical system is to employ a method in which the front lens group is a positive telephoto type and the back lens group is a negative telephoto type, and the power of each lens is increased. In this case, however, the exit angle of the edge rays emerging from the lens becomes greater than 20°, resulting in insufficient brightness at the edges. In addition, because the aberration correction for achieving the performance of the image-capturing device is too difficult, many aspherical surfaces must be used. In many cases, the final lens, in particular, must have a special shape: it must behave as a concave lens in the region close to the optical axis and as a convex lens towards the edges. The relative decentering sensitivity of each lens element is high, and the precision required for parts and assembly thus increases, which causes poorer yields, and has generally reached a critical level. In this study, we focused on simultaneously satisfying the demands for compactness and high performance in an image-capturing module using free-shaped surfaces, and we designed, fabricated, and evaluated a prototype. The prototype optical system we constructed was formed of two free-shaped prisms and had an optical thickness of 5.7 mm.

For fabrication, basic important parameters of the free-shaped prisms, for example, shape errors and decentering, must be evaluated in the same way as for standard coaxial optical systems. However, because the free-shaped prisms were formed of asymmetric surfaces located at arbitrary positions, it was not possible to measure the decentering with a standard conventional measurement method. Therefore, we developed techniques for simultaneously evaluating the relative positions and shape errors of each surface with high precision. Using these techniques, it was possible to improve the simulation precision of the optical performance of the free-shaped prisms, which could then be fed back to the fabrication process, allowing the accuracy of the finished form of the elements to be improved. In this paper, we describe design features, fabrication, measurement, and evaluation when using free-shaped surfaces in an image-capturing optical system.

2. FREE-SHAPED OPTICAL SYSTEM

Arranging the optical components in a line, as in the coaxial systems described above, is conflicts with the need to make them thinner; therefore, we made the system thinner by folding the optical path with a combination of reflecting

surfaces and refracting surfaces. Also, we minimized the number of optical components by imparting optical power also to the reflecting surfaces.

A folded optical system is effective in making the system thinner, but if curvature is applied to a reflecting surface to impart optical power, decentering aberrations occur at that surface [1]. The following types of aberrations are caused by decentering:

- off-axis astigmatism,
- off-axis coma,
- off-axis distortion, and
- off-axis tilting of the image plane.

These aberrations, which do not occur in a coaxial optical system, also occur at the center of the image plane corresponding to the on-axis position. Therefore, some means of properly correcting them is required in the folded optical system.

To reduce these decentering aberrations or to cancel out the aberrations at each surface, it is effective to use a rotationally asymmetric curved surface (free-shaped surface), represented by Eq. (1) below, at each reflecting and refracting surface:

$$z = \sum_{n=0}^{k} \sum_{m=0}^{n} C_{nm} x^m y^{n-m} \tag{1}$$

3. DESIGN

3.1 Specifications and Optical Design

The target specifications of the image-capturing optical system designed and investigated here are shown in Table 1.

Table 1 Target specifications

Sensor size	1/4inch
Focal length	3.6 mm, effective (equivalent in 35mm photography)
Fno	2.8, effective
Optical thickness	6.0 mm or less
Optical performance	compatible with 3 megapixels or above

Because the resolution of mobile-phone cameras has dramatically increased, we focus on the optical performance of 3 megapixel class modules and the our company's compact digital cameras.

We investigated various aspects of folded optical systems having optical performance compatible with 3 megapixels and above and capable of achieving thin modules, and as a result, we found that an optical system formed of two free-shaped prisms, as shown in Fig. 3, satisfies the required performance most satisfactorily. In addition, it can be made thinner than a coaxial system having the same optical performance.

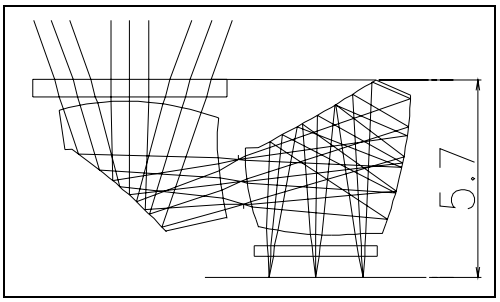

Fig. 3 Optical system using free-shaped prisms.

In this optical system, the incident beam from the object is reflected once in the first prism, is emitted towards the second prism, is reflected twice in the second prism, and forms an image on the image capturing surface. Because the aberrations are insufficiently corrected with a total of two reflections, and the back focus is too short with four reflections, performing three reflections, with two of them in the second prism, which has strong positive refractive power, is suitable for realizing a thin image-capturing optical system. An aperture stop is placed between the first prism and the second prism. The parallel flat plates in the figure represent cover glasses. All transmitting surfaces and reflecting surfaces in this optical system have optical power and are designed using free-shaped surfaces described by Eq. (1). Thus, by folding the optical path, we realized an optical system whose thickness was less than 6 mm.

3.2 Optical System Characteristics

(1) Use of retrofocus optical system

Considering the arrangement of powers in this optical system, it is a retrofocus type optical system including a negative group and a positive group in this order from the object side. Fig. 4 shows the arrangement of powers in the Y and X cross-sections of each surface in the optical system.

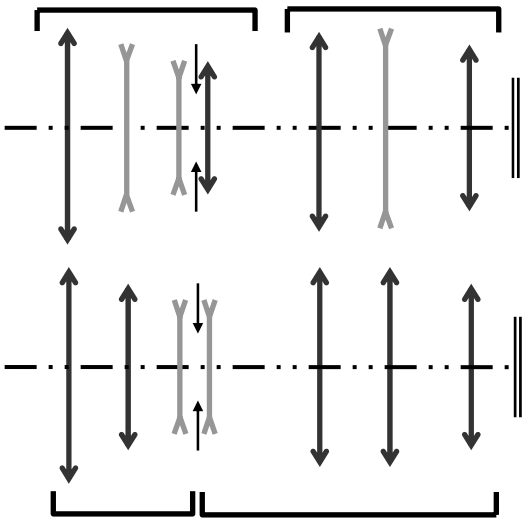

Fig. 4 Power arrangement of surfaces.

One characteristic of a retrofocus optical system is that the exit angle from the final optical surface is close to parallel for all image heights, which is an advantage because it produces more uniform image shading [3]. Generally, however, in this type of system, the total lens length is large compared with the focal length, which is a disadvantage in terms of achieving a thin optical system. This issue can be overcome by using a folded optical system. In addition, even though the thickness is reduced by folding the optical path, the total optical path length increases. Therefore, the powers of the individual surfaces can be reduced, which makes the level of the aberrations caused at each surface comparatively small, thus realizing an optical system with extremely high optical performance overall. Moreover, reducing the power at each surface is an advantage because it allows the error sensitivity to manufacturing variations to be reduced. Because the way in which decentering aberrations occur in this optical system is different in the Y direction and the X direction, another characteristic of the system is that it exhibits a noticeable difference in the arrangement of refractive powers in the YZ plane and in the XZ plane.

(2) Design for increasing powers of reflecting surfaces

A second characteristic of this optical system is that the powers of the reflecting surfaces are greater than those of the transmitting surfaces. By using the property that no chromatic aberrations occur at the reflecting surfaces, the chromatic aberrations of the whole optical system can be corrected to an extremely small level. In the case of a coaxial system, correction of chromatic aberrations is generally difficult if it is constructed of a small number of lenses. This is because monochromatic aberrations such as spherical aberrations can be corrected to some degree by using aspherical surfaces,

but chromatic aberrations can only be corrected by using a combination of different glasses. Particularly with plastic materials, it is usually not possible to select lens materials.

Because of this, we realized an optical system exhibiting both good compactness and optical performance by using free-shaped prisms. Fig. 5 shows MTF curves (design values) of the optical system.

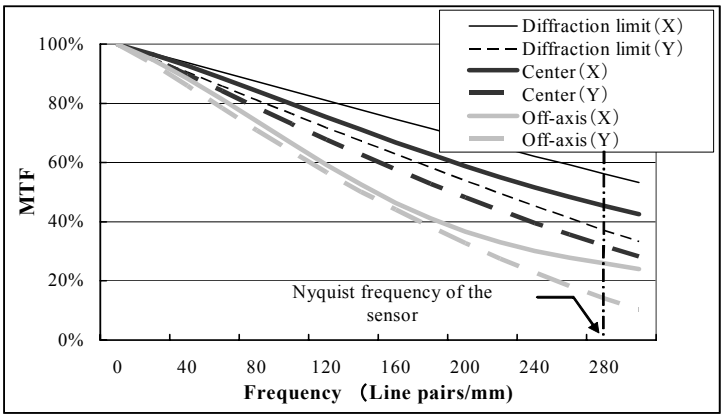

Fig. 5 Design MTF values. (Spatial frequency vs. MTF.)

Aberrations could be corrected to a reasonably high degree. The optical performance at the center of the image approached the diffraction limit, and even at the edges of the image, a resolution exceeding 200 lp/mm was possible. Thus, extremely high imaging performance was maintained from the center to the edges.

The system exhibits a Nyquist frequency corresponding to 3 megapixels, but it has sufficient optical performance to be compatible even with 4 megapixel image-capturing devices.

3.3 Fabrication Errors

The influence of variations in the optical surface precision, spacing between surfaces, decentering between surfaces, decentering and spacing between optical components, and the optical characteristics of the materials on the performance deterioration was the same as in a coaxial system. Fig. 6 shows the amount of deterioration when relative positional shifting errors occur during assembly of the first prism and the second prism.

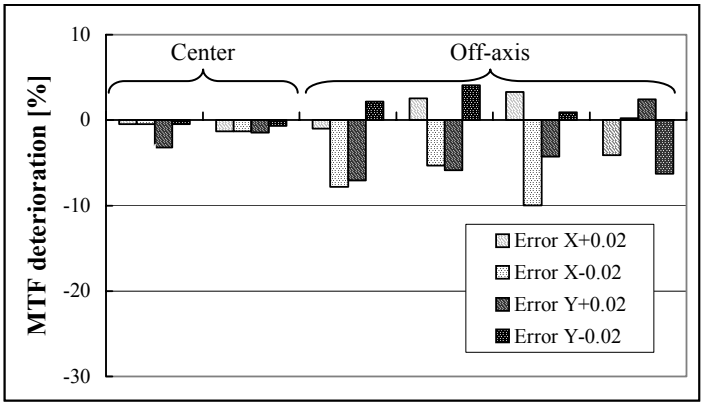

Fig. 6 MTF deterioration vs.assembly error.

The amount of decentering was 20 μm, the vertical axis shows MTF deterioration, and the evaluated positions were the center and the edge (70% of the image height). Even at positions where the MTF deterioration was maximum was less than 10%, indicating that the influence of assembly errors was comparatively small.

4. PROTOTYPE

We fabricated the two free-shaped prisms in the designed optical system using plastic molds. The prototype free-shaped prisms are shown in Fig. 7. After forming the prisms, mirror coatings were applied to the reflecting surfaces and antireflection (AR) coatings were applied to the refracting surfaces.

Fig. 7 Free-shaped prisms.

5. MEASUREMENT AND EVALUATION

5.1 Evaluation of Shape Errors

We measured the shapes of the effective area of each surface in the prototype prisms using a commercial ultrahigh-precision three-dimensional shape measuring device and evaluated the shape errors from the measurement results. The method, which is described below, was basically the same as a standard method used to evaluate axisymmetric aspherical lenses. First, to calculate positions in a local coordinate system from the measurement results, we calculated parameters for the coordinate conversion of the measurement data by optimization so as to minimize an evaluation function defined as a sum of squares of the residual error between the measured values and the designed shape (alignment processing), and we used the shape difference with respect to the design shape represented in the same coordinate system as the shape error. To evaluate the shape error quantitatively, we obtained rms values and peak-to-valley (P-V) values at the effective surfaces.

By modifying the shape of the mould so that the shape errors were cancelled, it was possible to finally reduce the P-V value of the shape error in the measurement region on each surface to 0.2 μm or less.

5.2 Evaluation of Decentering Error

Because the free-shaped prisms were configured so that each surface was decentered, it was difficult to measure the decentering error using a conventional method for measuring standard axisymmetric optical systems. Therefore, we developed a novel method for measuring the relative positions of each surface constituting the free-shaped prisms. In this method, we separately fabricated a glass block in which surfaces corresponding to the surfaces of the free-shaped prism to be designed were formed as planar surfaces. We measured the surface shapes of the glass block and the free-shaped prism together, and calculated the relative position of each surface of the free-shaped prism with reference to the measurement results of the glass block.

It was necessary to prepare individual glass blocks matching the shapes of the free-shaped prisms to be measured, and the angles formed by each surface of the fabricated glass blocks were measured with high precision in advance using a collimator. The free-shaped prism was fixed to a rotation stage so that the surfaces corresponding to those of the glass block were aligned (Fig. 8).

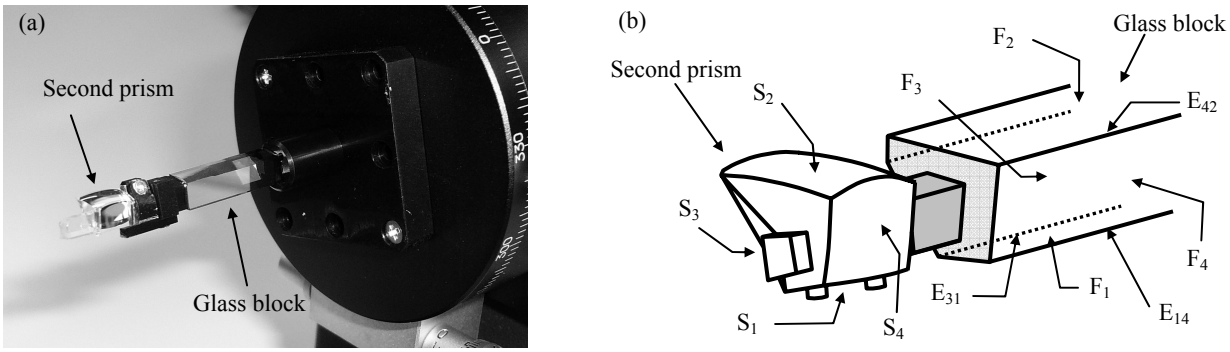

Fig. 8 (a) Photograph of second prism mounted to glass block. (b) Layout diagram of second prism and glass block. S1, S2, S3, S4: surfaces 1 to 4 of second free-shaped prism. F1, F2, F3, F4: surfaces 1 to 4 of glass block. E31: boundary between surface 3 and surface 1 of glass block. E14: boundary between surface 1 and surface 4 of glass block. E42: boundary between surface 4 and surface 2 of glass block.

During measurement, the surface being inspected was positioned using the rotation stage so as to be substantially orthogonal to the measurement probe, and using the commercial non-contact three-dimensional shape measurement device, the positions of edges of the boundary regions between the surface shape of measurement surfaces of the free-shaped prism and the surface shape of the glass block were measured. The measurement was performed in the same coordinate system. Only the edges of the boundary regions defined by planar surfaces corresponding to the effective surfaces of the free-shaped prism should be measured. Fig. 9 shows the shape measurement results of each surface of the second free-shaped prism, the planar surface shapes of the glass block, and the positions of the edges.

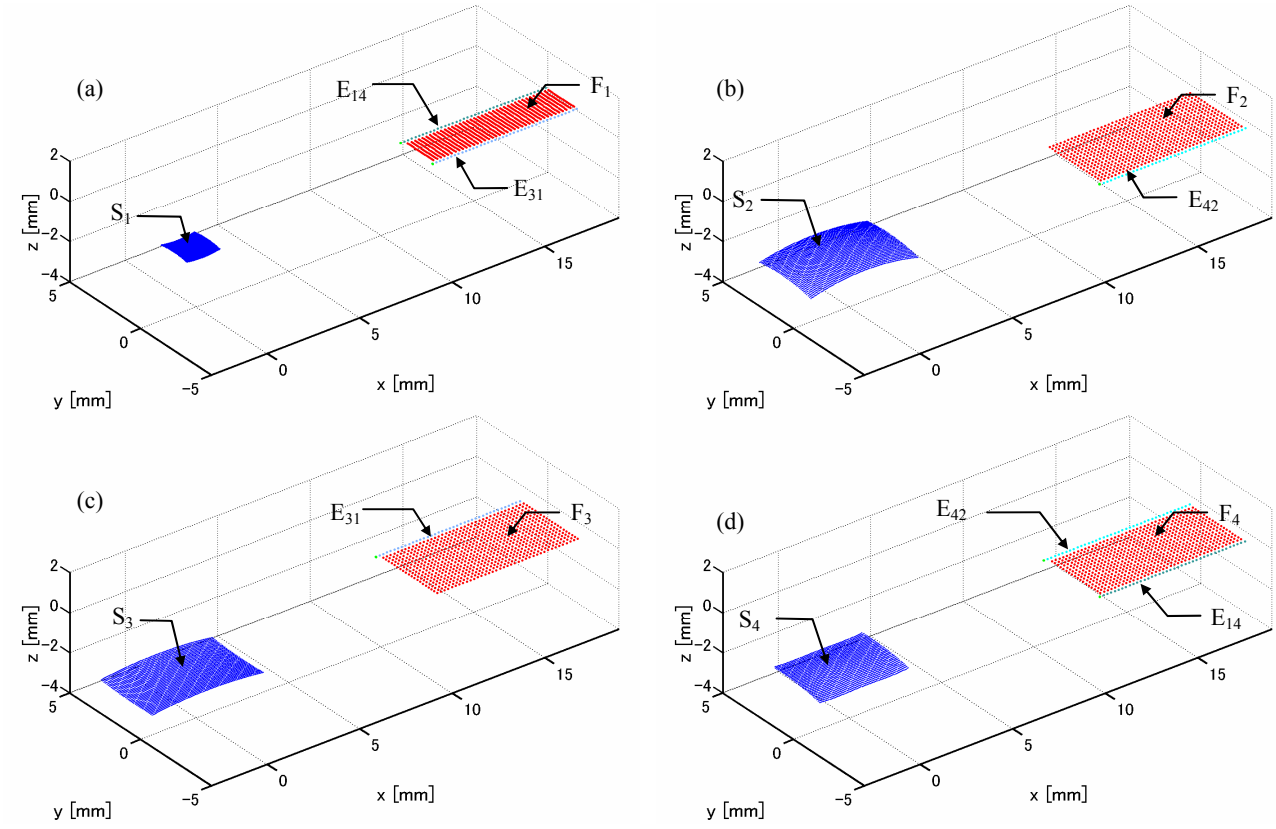

Fig. 9 Sample measurement results of each surface of the second prism, showing measurement results for (a) surface 1, (b) surface 2, (c) surface 3, and (d) surface 4.

We then performed the following analysis procedure using the measurement data for each surface.

(1) In the measurement data for each surface, the data for the edges of the glass block was approximated with a straight line, and the measurement data for the planar surface shapes was approximated with the equation of a plane.

(2) For the measurements of the common edges in the measurement data for each surface, we performed a coordinate transformation so that the straight line calculated in Step (1) was spatially aligned. We also performed this coordinate transformation for each data set measured in the same coordinate system and for the approximation calculated in Step (1) in the same way.

(3) Defining the straight line aligned in Step (2) as a rotation axis, we performed a rotational coordinate transformation so that the angle defined by each planar surface (the angle formed by the normal vector of the approximated equation of the plane) was aligned with the angle defined by the two planar surfaces measured in advance.

By performing this analysis for the other edges, we could modify the shape of the free-shaped prism. Fig. 10 shows the analysis results.

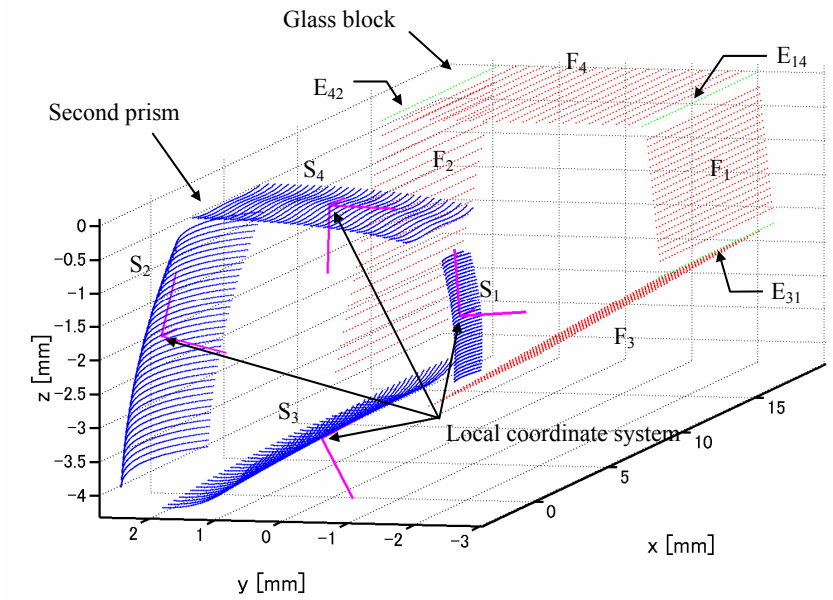

Fig. 10 Results of reconstructing the local coordinate system calculated from measurement results of each surface of the second prism and glass block.

By performing the alignment processing described in Section 5.1 on the surface shape measurement results of the free-shaped prism to calculate the positions in the local coordinate system, the relative positions in the local coordinate system of each surface can also be calculated by the same analysis. To quantitatively evaluate the decentering error, the decentering error (shift and tilt) of each surface was calculated to display the positions in the local coordinate systems of the other surfaces with reference to the local coordinate system of the specified surface and comparing them with the positions in the local coordinate system in the design values. As an example of this analysis, the results of the decentering errors (shifts: dx, dy, and dz [mm]; tilts: α, β, and γ [deg.]) of surfaces 2 to 4 of the second prism, with reference to surface 1, are summarized in Table 2. The reproducibilities of this method, in terms of 3σ, were about 5 μm and 2 arcmin.

Table 2 Measured values of shift and tilt. (dx, dy, dz: shift errors along x, y, and z axes in the local coordinate system of each surface [mm]. α, β, γ: tilt errors around x, y, and z axes in the local coordinate system of each surface [deg.])

	dx	dy	dz	α	β	γ
Surface 2	0.002	0.015	-0.001	0.083	-0.072	0.128
Surface 3	-0.027	-0.017	-0.004	-0.007	0.029	0.096
Surface 4	-0.018	0.018	0.004	0.028	0.054	0.056

It was possible to feed back the decentering errors to correct the positions of the mould used for forming the free-shaped prism. One feature of this method is its ability to calculate decentering errors and shape errors simultaneously by using the measured data. From these evaluation results, we found that it was possible to fabricate free-shaped prisms with sufficiently small errors, for both surface shape and decentering.

5.3 Simulation of Optical Performance

Using the method described in Section 5.2, it was possible to determine the decentering errors and the shape errors of the measurement sample. Therefore, it was possible to simulate the optical performance with high precision using these analysis results. Fig. 11 shows the MTF measurement results of the prototype optical system.

Fig. 11 shows simulated and measured MTF values at the center of the image and at a position located at 70% of the image height. The horizontal axis shows the amount of defocus (±0.05 mm), and the vertical axis shows the MTF value. The spatial frequencies evaluated were 30, 70, and 130 lp/mm. With the prototype free-shaped image-capturing module, it was possible to obtain a resolution close to the design performance.

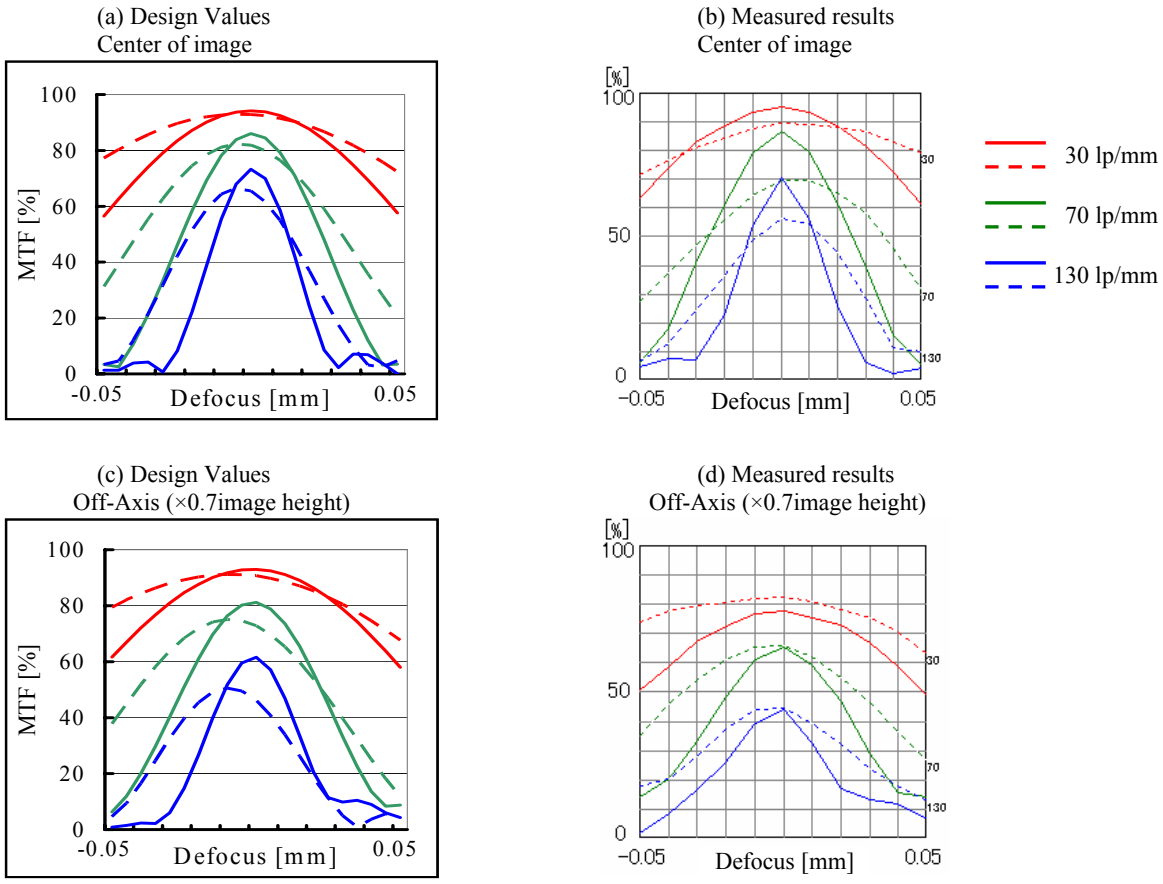

Fig. 11 MTF vs. defocus. (a) Design values at center. (b) Measured values at center. (c) Design values at 70% of image height. (d) Measured values at 70% of image height.

An image captured with the prototype optical system is shown in Fig. 12. We evaluated the image acquired with a 1.3 megapixels image-acquisition device. We obtained high resolution and good image quality, even at the edges of the image. Furthermore, it should also be possible to apply the optical system to 3 megapixels image-capturing devices.

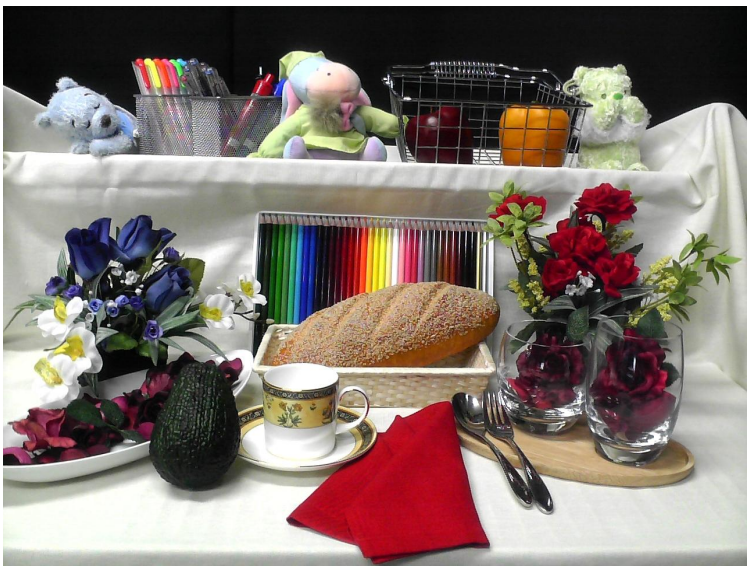

Fig. 12 Photograph using our camera module.

6. CONCLUSION

The development of free-shaped surfaces at Olympus started with their application to display optical systems; more recently, they have been fabricated for image-capturing optical systems, a purpose for which they have not been used until now. We confirmed that the prototype optical system had imaging performance close to the design values and described the practical evaluation of the prototype in thin, high-performance, ultracompact camera modules for which there is a demand.

In addition, we have been investigating the new concept of axially symmetric free-form lenses, and our studies are now proceeding. Example applications of axially symmetric free-form lenses (Fig. 13) include projectors that can project images in all directions (a horizontal angle of view of 360°) and a camera that can acquire images in all directions. We plan to continue investigating the potential of such free-form surfaces further.

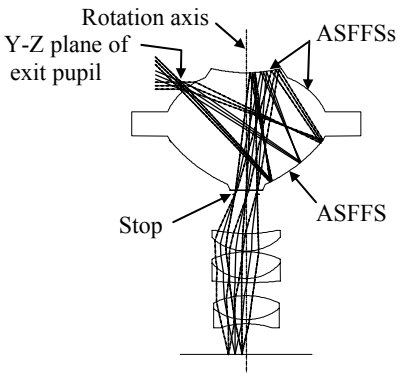

Fig. 13 Photograph and optical diagram of prototype axially symmetric free-form lens.
ASFFS: axially symmetric free-form surfaces.

REFERENCES

[1] T. Togino：Optical and Electro-Engineering Contact 39(**9**), 3-11 (2001)
http://www.olympus.co.jp/jp/news/1998a/nr980414fmdj.cfm

[2] For example T. Togino and T. Takeyama：US Patent 6,396,639

[3] S. Mihara：Optical and Electro-Engineering Contact 38(**9**), 21-28 (2000)

[4] http://www.olympus.co.jp/jp/news/2007b/nr070706zenhouij.cfm